ACS APPLIED MATERIALS & INTERFACES

www.acsami.org

Research Article

Synthesis of Wafer-Scale Monolayer Pyrenyl Graphdiyne on Ultrathin Hexagonal Boron Nitride for Multibit Optoelectronic Memory

Xing-Han Wang, Zhi-Cheng Zhang, Jing-Jing Wang, Xu-Dong Chen,* Bin-Wei Yao, Ya-Xin Hou, Mei-Xi Yu, Yuan Li, and Tong-Bu Lu*

Cite This: *ACS Appl. Mater. Interfaces* 2020, 12, 33069–33075

Read Online

ACCESS | Metrics & More | Article Recommendations | Supporting Information

ABSTRACT: Graphdiyne is a new two-dimensional carbon allotrope with many attractive properties and has been widely used in various applications. However, the synthesis of large-area, high-quality, and ultrathin (especially monolayer) graphdiyne and its analogues remains a challenge, hindering its application in optoelectronic devices. Here, a wafer-scale monolayer pyrenyl graphdiyne (Pyr-GDY) film is obtained on hexagonal boron nitride (hBN) via a van der Waals epitaxial strategy, and top-floating-gated multibit nonvolatile optoelectronic memory based on Pyr-GDY/hBN/graphene is constructed, using Pyr-GDY as a photoresponsive top-floating gate. Benefiting from the excellent charge trapping capability and strong absorption of the graphdiyne film, as well as the top-floating-gated structure and the ultrathin hBN film used in the device, the optoelectronic memory exhibits high storage performance and robust reliability. A huge difference in the current between the programmed and erased states (>26 μA μm^{-1} at V_{ds} = 0.1 V) and a prolonged retention time (>10^5 s) enable the device to achieve multibit storage, for which eight and nine distinct storage levels (3-bit) are obtained by applying periodic gate voltages and optical pulses in the programming and erasing processes, respectively. This work provides an important step toward realizing versatile graphdiyne-based optoelectronic devices in the future.

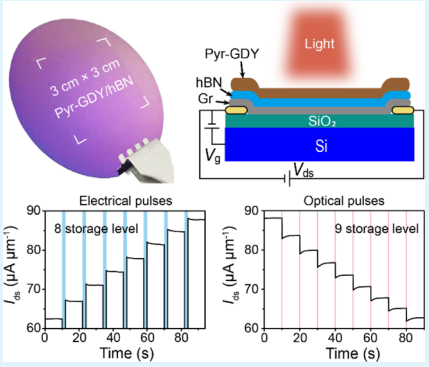

KEYWORDS: *monolayer pyrenyl graphdiyne, van der Waals epitaxy, photoresponsive top floating gate, multibit storage, nonvolatile optoelectronic memory*

1. INTRODUCTION

Graphdiyne (GDY), a new two-dimensional (2D) carbon allotrope containing only sp and sp^2 carbon atoms with high degrees of π-conjugation, has attracted tremendous attention because of its novel structure and outstanding properties.[1−5] The highly conjugated π-system, tunable intrinsic bandgap, strong optical absorption, and distinct electrical properties have lead to GDY and its analogues being widely applied in photo/electrocatalysis,[6−8] energy storage and conversion,[9−13] water purification,[14,15] and humidity sensors.[16] In particular, the predicted ultrahigh carrier mobilities and a natural bandgap[17−19] endow GDY with attractive prospects for electronic and optoelectronic applications. However, the applications of GDY in these fields, especially in optoelectronic memory, remain in their infancy. The major obstacle for further development lies in the fact that GDY films prepared via existing methods hardly satisfy the requirements of device applications. In recent years, many efforts have been made to prepare large-area and high-quality GDY and GDY analog films.[20−25] For example, an interface-confined synthetic strategy was developed to synthesize GDY[24,25] and N-GDY[23] films at the liquid/liquid or gas/liquid interfaces, and a solution-phase van der Waals epitaxial synthetic strategy was proposed to obtain highly crystalline and ultrathin GDY[20,21] and β-GDY[22] films on graphene. However, GDY films prepared via these methods are either very thick or difficult to exfoliate, which limits their further applications in optoelectronics. Until now, the synthesis of large-area and high-quality monolayer GDY and its analogues suitable for device applications has remained a challenge.

Promoting in-plane coupling and suppressing out-of-plane cross-linking of monomer molecules are key to obtaining a monolayer GDY film, and van der Waals epitaxy has been demonstrated to be an effective way to confine the in-plane growth of GDY.[20] In this work, wafer-scale monolayer pyrenyl graphdiyne (Pyr-GDY) was obtained on the hexagonal boron nitride (hBN) substrate by an Eglinton coupling reaction using

Received: March 22, 2020
Accepted: June 26, 2020
Published: June 26, 2020

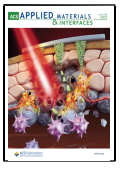

https://dx.doi.org/10.1021/acsami.0c05327
ACS Appl. Mater. Interfaces 2020, 12, 33069−33075

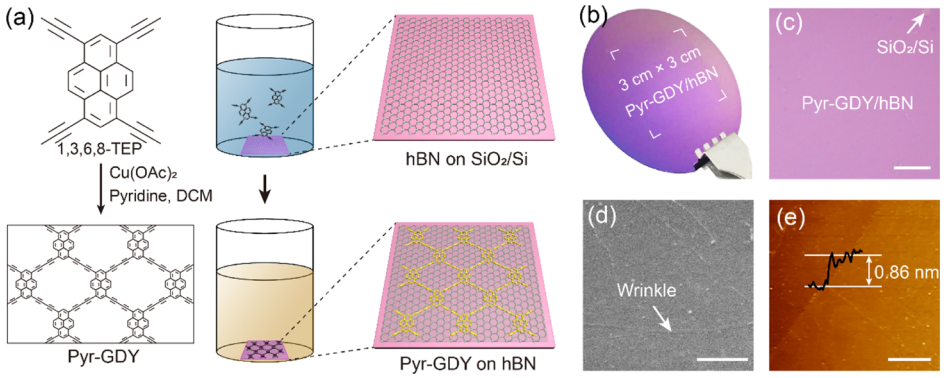

Figure 1. (a) Schematic illustration of the synthesis process of the Pyr-GDY film on hBN. (b) Photograph of a wafer-scale monolayer Pyr-GDY on hBN. (c,d) OM and SEM images of the as-prepared Pyr-GDY/hBN film on the SiO_2/Si substrate. Scale bar, 20 and 2 μm, respectively. (e) AFM image of the monolayer Pyr-GDY film on hBN. Scale bar, 2 μm.

1,3,6,8-tetraethynylpyrene (TEP) as monomers. Compared with the previously used graphene substrate, hBN is an ideal epitaxial substrate for the preparation of GDY for device applications because hBN has been widely used as a dielectric substrate in various devices, such as field effect transistors (FETs),[26] tunneling devices,[27] photodetectors,[28] artificial synapses,[29] and nonvolatile memories,[30−34] to improve device performance. Therefore, GDY and its analogues synthesized on the hBN film can be directly used for device applications without further exfoliation. In addition, we have found that GDY exhibits excellent charge-trapping capability in recent research, enabling its application in optoelectronic memory as a photoresponsive top-floating gate. Herein, we constructed a multibit optoelectronic memory with the structure of Pyr-GDY/hBN/graphene. This device can be programmed via a positive gate voltage, while the erasing process can be achieved by applying a negative gate voltage or by light illumination. Benefitting from the excellent charge-trapping capability of Pyr-GDY, an ultrathin hBN film (3 nm) can be used to separate the graphene channel and Pyr-GDY; this significantly improves the storage performance of the memory device, leading to a large memory window (137 V at $V_{g\text{-max}} = \pm 90$ V), the use of small programming/erasing voltages (± 30 V), and a small light pulse energy (3 nJ). The reliability and stability of the device are demonstrated from its long retention time ($>10^5$ s) and programing/erasing (P/E) endurance of 100 cycles. Moreover, the huge difference in currents between the programmed and erased states provides a route to achieve multibit storage, for which eight and nine distinct storage states (3-bit) are obtained by applying periodic electrical/optical pulses, respectively.

2. RESULTS AND DISCUSSION

Figure 1a schematically illustrates the synthesis process of a monolayer Pyr-GDY film on hBN using 1,3,6,8-TEP as monomers. First, a monolayer hBN film was grown onto Cu foil via chemical vapor deposition (CVD) and then transferred onto a SiO_2/Si substrate followed by thermal annealing (Figure S1). The as-prepared hBN epitaxial substrate was immersed into a pyridine solution of $Cu(OAc)_2$ and toluene in a reactor, followed by the slow addition of a CH_2Cl_2 solution of 1,3,6,8-TEP monomers into the reactor during the reaction using an injection pump. As the bending energy of 1,3,6,8-TEP monomers on hBN is higher than that on Pyr-GDY, the monomers prefer to adsorb onto hBN because of thermodynamics that favor the in-plane coupling reaction. Furthermore, to control the kinetics of the reaction, 1,3,6,8-TEP solution with an ultralow concentration (1 μM) was slowly injected into the solution mixture at a rate of 10 μL min^{-1} to avoid the accumulation of monomers on hBN. After 24 h successive reaction in an Ar atmosphere and dark environment at room temperature, a monolayer Pyr-GDY film was synthesized on hBN. As shown in Figure 1b, a wafer-scale monolayer Pyr-GDY film was obtained on the hBN film. As shown in Figure 1c,d, optical microscopy (OM) and scanning electron microscopy (SEM) images demonstrate that the as-prepared Pyr-GDY film on hBN is continuous and uniform. The wrinkles marked in Figure 1d originate from the growth and transfer processes of the hBN film.[35,36] Atomic force microscopy (AFM) characterization shows that the total thickness of the Pyr-GDY/hBN film is approximately 0.86 nm (Figure 1e), indicating that a monolayer Pyr-GDY film is obtained via this method. The thickness of the Pyr-GDY film can be controlled by adjusting the concentration of the monomer solution. Figure S6 shows a three-layer Pyr-GDY film on hBN prepared using a monomer solution with a concentration of 2 μM during the reaction.

The bonding structure and chemical composition of Pyr-GDY on hBN were investigated by Raman spectroscopy and X-ray photoelectron spectroscopy (XPS). As shown in Figure 2a, six sharp Raman bands at 1247, 1368, 1499, 1609, 2104, and 2193 cm^{-1} were observed in the Raman spectrum of the Pyr-GDY/hBN film. The band at 1247 cm^{-1} is attributed to the C−H in-plane bending vibration, while the bands at 1368, 1499, and 1609 cm^{-1} are ascribed to the C═C stretching vibration of the pyrene rings.[37] Especially, the remarkable bands at 2104 and 2193 cm^{-1} correspond to the in-plane and out-of-plane stretching vibration of C≡C triple bonds, respectively, indicating high crystallinity for the as-prepared Pyr-GDY film.[20] The Raman band for the hBN film at 1369 cm^{-1} is very weak (Figure S2)[38] and is covered by the band at 1368 cm^{-1}. The XPS spectrum in Figures S7 and 2b indicate that the primary element comprising the Pyr-GDY film is carbon and that the C 1s peak can be deconvoluted into four subpeaks at 284.6, 285.3, 286.7, and 288.5 eV, corresponding to C═C, C≡C, C−O, and C═O bonds, respectively.[20−22] The experimentally observed ratio for the C≡C and C═C bands was 1:2, which is consistent with the theoretical ratio for the sp- and sp^2-hybridized carbon atoms in Pyr-GDY. In addition, the small C−O and C═O bands relative to those found for the GDY films in previous studies indicate the high

https://dx.doi.org/10.1021/acsami.0c05327
ACS Appl. Mater. Interfaces 2020, 12, 33069−33075

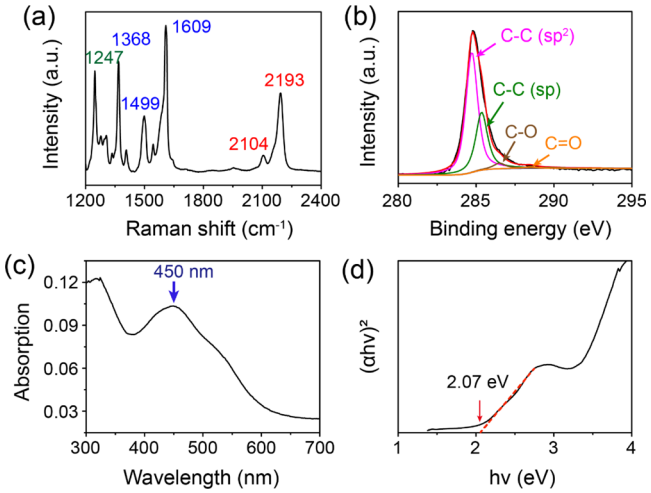

Figure 2. (a) Raman spectrum of the as-prepared Pyr-GDY film on hBN. (b) High-resolution XPS of C 1s. (c) UV−vis absorption spectrum of the as-prepared Pyr-GDY film. (d) Tauc plot of the Pyr-GDY film.

quality of the prepared Pyr-GDY film.[20] The absorption of the Pyr-GDY was characterized via UV−vis absorption spectroscopy, which exhibited a strong absorption peak at 450 nm (Figure 2c). The nonzero absorption of the Pyr-GDY film at longer wavelengths, which was also observed in previous studies,[21,39] may originates from the disordered defects embedded in the Pyr-GDY film. The Tauc plot shown in Figure 2d indicates that the bandgap of Pyr-GDY on hBN is 2.07 eV, which is larger than that of the multilayer GDY film (~1.4 eV).[21,39] The larger bandgap, which is attributed to the smaller π-electron delocalization and the monolayer thickness of Pyr-GDY,[40−42] will facilitate the separation of photogenerated electron−hole pairs, leading to a stronger photoresponse.

GDY has been predicted to show an ultrahigh carrier mobility comparable to that of graphene. However, a solution-phase synthetic strategy makes it difficult to synthesize ideal single-crystalline GDY. In fact, the prepared GDY films are polycrystalline with domains that are less than a few hundred nanometers in size, and the grain boundaries and disordered defects between domains seriously limit the carrier mobilities and conductivities. The electrical properties of the prepared monolayer Pyr-GDY film were investigated, and as shown in Figure S8, the results indicate a p-type behavior for the Pyr-GDY film with a carrier mobility and conductivity of 4.96 $cm^2 V^{-1} s^{-1}$ and 2.05×10^4 S m^{-1}, respectively, which are comparable to those found for GDY films in previous studies.[20,21,39,43]

The strong absorption and natural bandgap of Pyr-GDY enable its applications in optoelectronic devices. Here, we constructed a top-floating-gated multibit optoelectronic memory based on a Pyr-GDY/hBN/graphene heterostructure, as shown in Figure 3a. In this device, CVD-grown graphene and hBN films were used as the channel and dielectric layer, respectively, while a Pyr-GDY film synthesized on top of hBN served as a photoresponsive top-floating gate.[20] Details for the device fabrication are described in the Experimental Section and Figure S9. In nonvolatile memories, the thickness of the dielectric layer (hBN in this device) is very important for achieving high storage performance because a thicker dielectric film will suppress the tunneling of charges and degrade the device performance.[31] In our device, Pyr-GDY with abundant charge trapping sites can provide a higher density of charge storage and prevent the escape of trapped charges back to the graphene channel. As a result, a much thinner hBN film (3 nm) can be used in comparison with that used in the reported floating-gated memories.[31,32,44−46]

To demonstrate the data storage capability of the fabricated memory device, the transfer characteristics under different maximum gate voltages ($V_{g\text{-}max}$) were explored. As shown in Figure 3b, when the back-gate voltage V_g was swept from negative to positive and then back to negative, a bistable state regime originating from the obvious hysteresis was obtained, which is essential for the operation of a nonvolatile memory device. Moreover, the storage performance of a memory device can be estimated from the memory window (ΔV), which is defined as the difference in the gate voltage between the hysteresis curves marked in Figure 3b. As shown in Figure 3c, the memory window is 22 V when the gate voltage sweeps from −20 to 20 V and back to −20 V, which gradually broadens to 137 V with increasing $V_{g\text{-}max}$ to ±90 V, originating from the increase in the number of trapped charges in the Pyr-GDY film. It is worth noting that the absence of the ambipolar originates from the high top gate voltage (V_{tg}) induced by the trapped electrons in top-floating Pyr-GDY, which can effectively offset the applied positive back-gate voltage (Supporting Information Note 3). Benefitting from the ultrathin dielectric layer (3 nm hBN), the memory window of the Pyr-GDY/hBN/graphene-based memory is larger than that reported in previous results.[32,47] Control experiments were performed by measuring the electrical behavior of devices without a top-floating Pyr-GDY (Figures S10−12) or using a much thicker hBN film as the dielectric layer (Figure S13). Seriously degenerated storage performance was observed in the

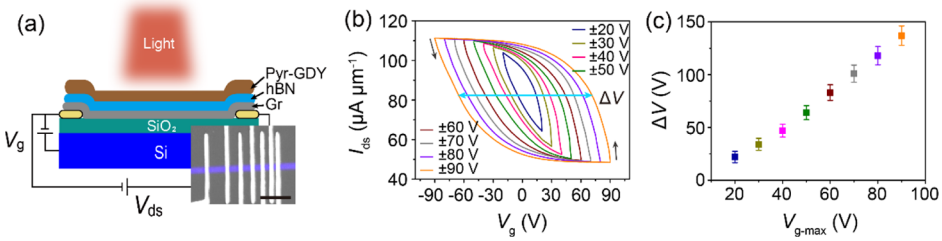

Figure 3. (a) Schematic illustration of the top-floating-gated optoelectronic memory based on the Pyr-GDY/hBN/graphene heterostructure. Inset is the false-colored SEM image of the fabricated device with different channel lengths. Scale bar, 20 μm. (b) Transfer curves of the memory device under different maximum gate voltage ($V_{g\text{-}max}$) ranging from ±20 to ±90 V at V_{ds} = 0.1 V. (c) Memory window (ΔV) as a function of the maximum gate voltage ($V_{g\text{-}max}$) extracted from (b). The effective length and width of the device were 5 and 6 μm, respectively.

https://dx.doi.org/10.1021/acsami.0c05327
ACS Appl. Mater. Interfaces 2020, 12, 33069−33075

control experiments, demonstrating that the excellent storage capability of the device is attributed to the top-floating Pyr-GDY and ultrathin hBN film.

Two resistance-switching cycles, including electrical programming, on-current reading, electrical/optical erasing, and off-current reading, are shown in Figure 4a. Small programming/erasing voltages are desirable for memory arrays in practical applications. A higher gate voltage is always required to effectively promote the tunneling of electrons through a thicker dielectric layer. In our device, an ultrathin hBN film (3 nm) is used as the dielectric layer, which is much thinner than that used in the reported optoelectronic memories with a similar structure,[31,32] enabling the gate voltage pulses with a smaller magnitude and shorter duration to be used to switch the on/off states of the device. For instance, after a positive V_g pulse (+30 V, 10 s, section I), the graphene channel was programmed from the off state to the on state; in turn, the device returned to its off state after a negative V_g pulse (−30 V, 10 s, section II). Owing to the strong absorption of the top-floating Pyr-GDY film, the erasing process can also be triggered by a weak light illumination (450 nm, 10 mW cm^{-2}, 1 s, section III), corresponding to a light energy of 3 nJ (according to a device area of ∼30 μm^2).

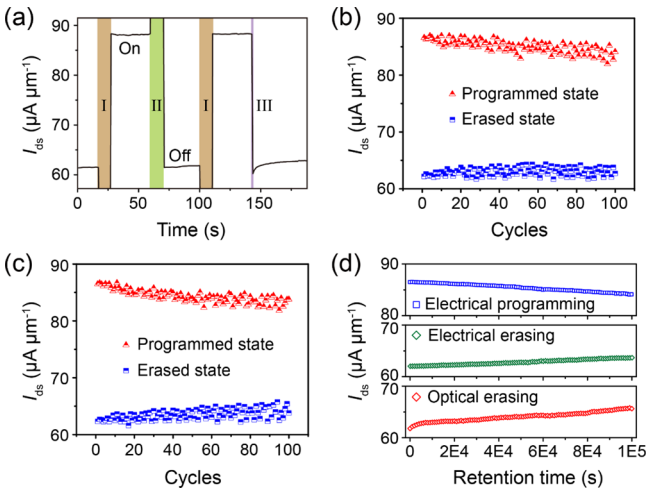

Figure 4. (a) Two resistance-switching cycles of the Pyr-GDY/hBN/graphene-based optoelectronic memory. V_g = ±30 V with a duration of 10 s was used for electrical programming (section I) and erasing (section II), and a 450 nm optical pulse (10 mW cm^{-2}, 1 s, section III) was used for optical erasing. The V_{ds} and V_g at current-reading and optical erasing processes were set to 0.1 and 0 V, respectively. (b,c) Current variation of the device at the programmed and erased states from the initial to 100 P/E cycles. The erasing processes are triggered by (b) electrical pulses and (c) optical pulses. (d) Retention characteristics of the device at the electrical programmed state (blue), electrical erased state (green), and optical erased state (red).

To demonstrate the reliability of the Pyr-GDY/hBN/graphene-based optoelectronic memory, the cyclic P/E endurance and retention time of the device were tested. Figure 4b,c show the current variation of the memory at the programmed and erased states from the initial to 100 P/E cycles using electrical pulses (−30 V, 10 s) and optical pulses (450 nm, 10 mW cm^{-2}, 1 s) for erasing processes, respectively. The currents are almost unchanged during the successive operations of electrical programming/electrical erasing (Figure 4b) and electrical programming/optical erasing (Figure 4c), indicating high durability and reliability of the Pyr-GDY/hBN/graphene-based optoelectronic memory. Moreover, high stability and endurance of the device were demonstrated via a long retention time of over 10^5 s (Figure 4d). The reduction of the on current with electrical programming (blue) was 2.4 μA μm^{-1} (2.8%) even after 10^5 s, while the off currents triggered by the electrical/optical pulses increased by 1.6 μA μm^{-1} (2.6%, green) and 4 μA μm^{-1} (6.4%, red). The high reliability and stability of our device can be attributed to the excellent charge-trapping capability of Pyr-GDY and the top-floating-gated structure and the high potential barrier induced by the hBN film.[31,48] The storage performance of the device triggered by ±90 V gate pulses was also investigated. As shown in Figure S14, a much larger current difference between the on- and off-current (50 μA μm^{-1}) was obtained by applying ±90 V gate pulses, while the retention characteristics of the device were slightly degenerated.

The mechanism for the programing and erasing processes is illustrated in Figure 5. The graphene channel is p-doped at the initial state as it is affected by the adsorbed molecules from ambient air, such as H_2O and O_2.[49] As illustrated in Figure 5a, while applying a gate voltage of +30 V for electrical programming, the Fermi level of graphene is elevated, and simultaneously, electrons from graphene will tunnel to the Pyr-GDY film through the hBN layer via the Fowler−Nordheim mechanism.[31,32,50] After the V_g pulse, these electrons are trapped in the Pyr-GDY because of the charge-trapping capability of the Pyr-GDY film and the potential barrier caused by the hBN. Consequently, the Pyr-GDY film can be regarded as a negatively charged top gate to the p-doped graphene channel, which will induce a sharp increase in the drain current I_{ds} to 88 μA μm^{-1} (programmed-state current). In contrast, while applying a −30 V gate voltage pulse for electrical erasing, a significant decrease in the graphene Fermi

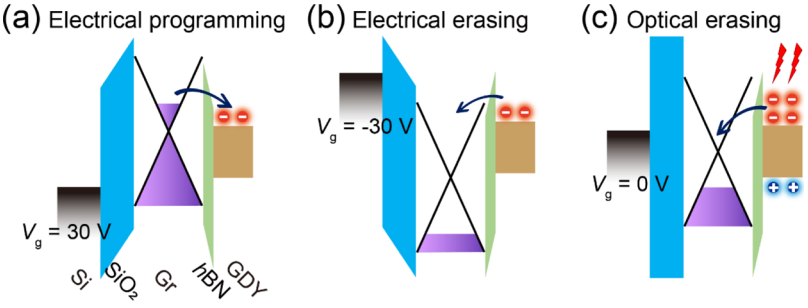

Figure 5. Schematic illustration of the energy band diagram of the memory device for (a) electrical programming, (b) electrical erasing, and (c) optical erasing.

https://dx.doi.org/10.1021/acsami.0c05327
ACS Appl. Mater. Interfaces 2020, 12, 33069−33075

level will induce a strong built-in electric field from the top-floating Pyr-GDY to the graphene channel, which will promote the tunneling of the trapped electrons in the Pyr-GDY film back to the graphene channel (Figure 5b). Accompanied by a release of trapped electrons in the top-floating gate, the negative top gate voltage will be removed and the device will return to its initial state with I_{ds} = 62 μA μm^{-1} (erased-state current).

The optical erasing process is illustrated in Figure 5c, in which abundant electron−hole pairs are generated in Pyr-GDY under illumination by a 450 nm light pulse. Driven by the built-in electric field between graphene and Pyr-GDY, the photogenerated electrons tunnel through the small triangular electron barrier to the graphene channel, whereas the photogenerated holes are blocked in the Pyr-GDY film by the large hole barrier between Pyr-GDY and hBN.[31,34] These holes neutralize the residual electrons trapped in the Pyr-GDY film and eliminate the negative gate bias to the graphene channel, resulting in recovery of the device to its erased state.

The huge current difference between the programmed and erased states of the device and the long retention time enable the optoelectronic memory to achieve multilevel electrical/optical data storage. Here, periodic electrical/optical pulses were used to trigger stepwise I_{ds} for distinct storage states. In the electrical programming process, the number of accumulated electrons in the top-floating Pyr-GDY film increases with the applied V_g pulses, which leads to a stepwise increase in the negative top gate voltage and I_{ds}. As shown in Figure 6a, eight

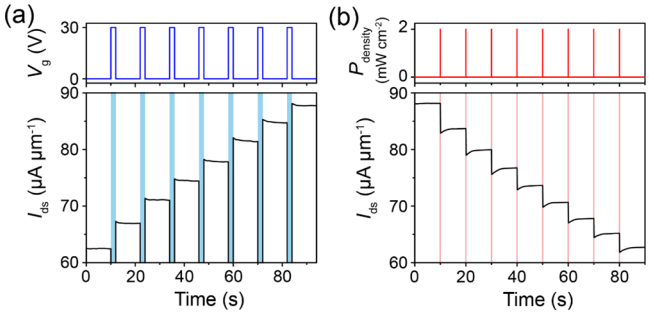

Figure 6. (a) I_{ds}−time curve under periodic gate voltage pulses (V_g = 30 V, t = 2 s), showing eight distinct storage states. (b) I_{ds}−time curve under 450 nm light pulses (P = 10 mW cm^{-2}, t = 0.2 s) every 10 s, achieving nine memory levels.

distinct current levels are achieved by applying periodic V_g pulses (30 V, 2 s). For the optical erasing process, periodic optical pulses will gradually neutralize the trapped electrons in the Pyr-GDY film, resulting in a stepwise decrease in the induced negative top gate voltage and drain current I_{ds}. Figure 6b shows the multilevel I_{ds} recorded under the periodic illumination of nine light pulses (10 mW cm^{-2}, 0.2 s) at V_{ds} = 0.1 V. Although eight and nine storage states have been demonstrated by applying a periodic gate voltage and light pulses, respectively, the difference in I_{ds} between neighboring current levels is still more than 2.6 μA μm^{-1}, which is much larger than the background noise (33 nA); therefore, more storage states can be obtained by carefully adjusting the intensity and duration of the electrical/optical pulses (Supporting Information Note 7). As shown in Figure S15, two distinct current levels with a gap of 35 nA were obtained by applying a gate pulse with a magnitude of 30 V for a duration of 100 ms, indicating that more than 740 storage levels can be obtained.

3. CONCLUSIONS

In summary, a wafer-scale monolayer Pyr-GDY film was prepared on a hBN film using a van der Waals epitaxial strategy. The Pyr-GDY/hBN heterostructure can be directly used in various devices, and a top-floating-gated multibit optoelectronic memory based on the Pyr-GDY/hBN/graphene heterostructure was constructed and studied in this work, which used a Pyr-GDY film as a photoresponsive top floating gate. Owing to the excellent charge-trapping capability and strong absorption of the Pyr-GDY film and the top-floating-gated structure and ultrathin dielectric layer of the device, high storage performance was achieved for both electrical and optical operations, resulting in a large memory window (137 V at $V_{g\text{-}max}$ = ±90 V), the use of small programming/erasing gate voltages (±30 V), and a small light pulse energy (3 nJ). The device exhibited high reliability and stability with a retention time exceeding 10^5 s and a P/E endurance of >100 cycles. The huge difference in current between the programmed and erased states and the long retention time enable the device to achieve multibit storage. Eight distinct storage levels were obtained by applying periodic V_g pulses in the programming process, while treatment with periodic optical pulses can be used to generate nine current stages in the erasing process. Our work demonstrates that GDY and its analogues are promising candidates for application of nonvolatile optoelectronic memory, paving the way for the development of GDY-based optoelectronic devices.

4. EXPERIMENTAL SECTION

4.1. Synthesis of Wafer-Scale Monolayer Pyr-GDY. A 3 cm × 3 cm CVD-grown monolayer hBN film was transferred onto a 2 in. SiO_2/Si wafer and then annealed at 350 °C for 3 h in an atmosphere of flowing Ar (90 sccm) and H_2 (10 sccm) to obtain a clean and flat surface. After annealing, the hBN film was immersed into 50 mL pyridine solution of $Cu(OAc)_2$ (2 mM) and 20 mL of toluene in a homemade reaction vessel. Then, 50 mL CH_2Cl_2 solution of 1,3,6,8-TEP monomer (1 μM) was slowly injected into the reactor using an injection pump at a rate of 10 μL min^{-1}. After 24 h successive catalytic coupling reaction in an Ar atmosphere and dark environment at room temperature, a wafer-scale monolayer Pyr-GDY film was obtained on hBN.

4.2. Device Fabrication. The source and drain electrodes (Cr/Au 10/50 nm) of the device were first fabricated on a 285 nm SiO_2/Si substrate by laser-direct lithography (miDALIX) and thermal evaporation. A single-crystalline monolayer graphene film and a hBN film with a thickness of 3 nm were vertically stacked on the Cr/Au electrodes, and then, the hBN/graphene heterostructure was patterned into the rectangular channel by laser-direct lithography and oxygen plasma etching. Before Pyr-GDY synthesis, the sample was annealed at 350 °C for 3 h to get a clean surface and a close contact between graphene and electrodes. Finally, a uniform Pyr-GDY film was synthesized on the hBN surface using the abovementioned method. In this work, the effective length and width of the device we measured were 5 and 6 μm, respectively.

■ ASSOCIATED CONTENT

Supporting Information

The Supporting Information is available free of charge at https://pubs.acs.org/doi/10.1021/acsami.0c05327.

Experimental details including the preparation of hBN, graphene, and 1,3,6,8-TEP monomers; AFM images of monolayer hBN and multilayer Pyr-GDY/hBN films;

https://dx.doi.org/10.1021/acsami.0c05327
ACS Appl. Mater. Interfaces 2020, 12, 33069−33075

Raman spectra of monolayer hBN and graphene; XPS spectrum of the Pyr-GDY film on hBN; device fabrication procedures; and the control experiments (PDF)

AUTHOR INFORMATION

Corresponding Authors

Xu-Dong Chen − *MOE International Joint Laboratory of Materials Microstructure, Institute for New Energy Materials and Low Carbon Technologies, School of Material Science and Engineering, Tianjin University of Technology, Tianjin 300384, China*; orcid.org/0000-0002-0184-3953; Email: chenxd@email.tjut.edu.cn

Tong-Bu Lu − *MOE International Joint Laboratory of Materials Microstructure, Institute for New Energy Materials and Low Carbon Technologies, School of Material Science and Engineering, Tianjin University of Technology, Tianjin 300384, China*; orcid.org/0000-0002-6087-4880; Email: lutongbu@tjut.edu.cn

Authors

Xing-Han Wang − *MOE International Joint Laboratory of Materials Microstructure, Institute for New Energy Materials and Low Carbon Technologies, School of Material Science and Engineering, Tianjin University of Technology, Tianjin 300384, China*

Zhi-Cheng Zhang − *MOE International Joint Laboratory of Materials Microstructure, Institute for New Energy Materials and Low Carbon Technologies, School of Material Science and Engineering, Tianjin University of Technology, Tianjin 300384, China*

Jing-Jing Wang − *MOE International Joint Laboratory of Materials Microstructure, Institute for New Energy Materials and Low Carbon Technologies, School of Material Science and Engineering, Tianjin University of Technology, Tianjin 300384, China*

Bin-Wei Yao − *MOE International Joint Laboratory of Materials Microstructure, Institute for New Energy Materials and Low Carbon Technologies, School of Material Science and Engineering, Tianjin University of Technology, Tianjin 300384, China*

Ya-Xin Hou − *MOE International Joint Laboratory of Materials Microstructure, Institute for New Energy Materials and Low Carbon Technologies, School of Material Science and Engineering, Tianjin University of Technology, Tianjin 300384, China*

Mei-Xi Yu − *MOE International Joint Laboratory of Materials Microstructure, Institute for New Energy Materials and Low Carbon Technologies, School of Material Science and Engineering, Tianjin University of Technology, Tianjin 300384, China*

Yuan Li − *MOE International Joint Laboratory of Materials Microstructure, Institute for New Energy Materials and Low Carbon Technologies, School of Material Science and Engineering, Tianjin University of Technology, Tianjin 300384, China*

Complete contact information is available at: https://pubs.acs.org/10.1021/acsami.0c05327

Author Contributions

X.-D.C. and T.-B.L. designed the project. X.-H.W. prepared the hBN and graphene films. J.-J.W. synthesized the Pyr-GDY film. X.-H.W., Z.-C.Z., and B.-W.Y. constructed the devices and performed the electrical measurements. X.-H.W., Y.-X.H., M.-X.Y., and Y.L. performed the characterizations. X.-D.C. wrote the manuscript. All authors discussed the results and revised the manuscript.

Funding

This work was supported by the NSFC (21790052, 51802220) and Natural Science Foundation of Tianjin City (19JCYBJC17300).

Notes

The authors declare no competing financial interest.

REFERENCES

(1) Li, G.; Li, Y.; Liu, H.; Guo, Y.; Li, Y.; Zhu, D. Architecture of Graphdiyne Nanoscale Films. *Chem. Commun.* **2010**, *46*, 3256−3258.

(2) Huang, C.; Li, Y.; Wang, N.; Xue, Y.; Zuo, Z.; Liu, H.; Li, Y. Progress in Research into 2D Graphdiyne-Based Materials. *Chem. Rev.* **2018**, *118*, 7744−7803.

(3) Gao, X.; Liu, H.; Wang, D.; Zhang, J. Graphdiyne: Synthesis, Properties, and Applications. *Chem. Soc. Rev.* **2019**, *48*, 908−936.

(4) Wu, L.; Dong, Y.; Zhao, J.; Ma, D.; Huang, W.; Zhang, Y.; Wang, Y.; Jiang, X.; Xiang, Y.; Li, J.; Feng, Y.; Xu, J.; Zhang, H. Kerr Nonlinearity in 2D Graphdiyne for Passive Photonic Diodes. *Adv. Mater.* **2019**, *31*, 1807981.

(5) Li, Y.; Xu, L.; Liu, H.; Li, Y. Graphdiyne and Graphyne: From Theoretical Predictions to Practical Construction. *Chem. Soc. Rev.* **2014**, *43*, 2572−2586.

(6) Yin, X.-P.; Wang, H.-J.; Tang, S.-F.; Lu, X.-L.; Shu, M.; Si, R.; Lu, T.-B. Engineering the Coordination Environment of Single-Atom Platinum Anchored on Graphdiyne for Optimizing Electrocatalytic Hydrogen Evolution. *Angew. Chem., Int. Ed.* **2018**, *57*, 9382−9386.

(7) Wang, S.; Yi, L.; Halpert, J. E.; Lai, X.; Liu, Y.; Cao, H.; Yu, R.; Wang, D.; Li, Y. A Novel and Highly Efficient Photocatalyst Based on P25-Graphdiyne Nanocomposite. *Small* **2012**, *8*, 265−271.

(8) Li, J.; Xie, Z.; Xiong, Y.; Li, Z.; Huang, Q.; Zhang, S.; Zhou, J.; Liu, R.; Gao, X.; Chen, C.; Tong, L.; Zhang, J.; Liu, Z. Architecture of β-Graphdiyne-Containing Thin Film Using Modified Glaser−Hay Coupling Reaction for Enhanced Photocatalytic Property of TiO_2. *Adv. Mater.* **2017**, *29*, 1700421.

(9) Huang, C.; Zhang, S.; Liu, H.; Li, Y.; Cui, G.; Li, Y. Graphdiyne for High Capacity and Long-Life Lithium Storage. *Nano Energy* **2015**, *11*, 481−489.

(10) Lu, C.; Yang, Y.; Wang, J.; Fu, R.; Zhao, X.; Zhao, L.; Ming, Y.; Hu, Y.; Lin, H.; Tao, X.; Li, Y.; Chen, W. High-Performance Graphdiyne-Based Electrochemical Actuators. *Nat. Commun.* **2018**, *9*, 752.

(11) He, J.; Wang, N.; Cui, Z.; Du, H.; Fu, L.; Huang, C.; Yang, Z.; Shen, X.; Yi, Y.; Tu, Z.; Li, Y. Hydrogen Substituted Graphdiyne as Carbon-Rich Flexible Electrode for Lithium and Sodium Ion Batteries. *Nat. Commun.* **2017**, *8*, 1172.

(12) Yang, Z.; Shen, X.; Wang, N.; He, J.; Li, X.; Wang, X.; Hou, Z.; Wang, K.; Gao, J.; Jiu, T.; Huang, C. Graphdiyne Containing Atomically Precise N Atoms for Efficient Anchoring of Lithium Ion. *ACS Appl. Mater. Interfaces* **2019**, *11*, 2608−2617.

(13) He, J.; Wang, N.; Yang, Z.; Shen, X.; Wang, K.; Huang, C.; Yi, Y.; Tu, Z.; Li, Y. Fluoride Graphdiyne as a Free-Standing Electrode Displaying Ultra-Stable and Extraordinary High Li Storage Performance. *Energy Environ. Sci.* **2018**, *11*, 2893−2903.

(14) Gao, X.; Zhou, J.; Du, R.; Xie, Z.; Deng, S.; Liu, R.; Liu, Z.; Zhang, J. Robust Superhydrophobic Foam: A Graphdiyne-Based Hierarchical Architecture for Oil/Water Separation. *Adv. Mater.* **2016**, *28*, 168−173.

(15) Li, J.; Chen, Y.; Gao, J.; Zuo, Z.; Li, Y.; Liu, H.; Li, Y. Graphdiyne Sponge for Direct Collection of Oils from Water. *ACS Appl. Mater. Interfaces* **2019**, *11*, 2591−2598.

(16) Yan, H.; Guo, S.; Wu, F.; Yu, P.; Liu, H.; Li, Y.; Mao, L. Carbon Atom Hybridization Matters: Ultrafast Humidity Response of Graphdiyne Oxides. *Angew. Chem., Int. Ed.* **2018**, *57*, 3922−3926.
(17) Long, M.; Tang, L.; Wang, D.; Li, Y.; Shuai, Z. Electronic Structure and Carrier Mobility in Graphdiyne Sheet and Nanoribbons: Theoretical Predictions. *ACS Nano* **2011**, *5*, 2593−2600.
(18) Koo, J.; Huang, B.; Lee, H.; Kim, G.; Nam, J.; Kwon, Y.; Lee, H. Tailoring the Electronic Band Gap of Graphyne. *J. Phys. Chem. C* **2014**, *118*, 2463−2468.
(19) Yue, Q.; Chang, S.; Kang, J.; Qin, S.; Li, J. Mechanical and Electronic Properties of Graphyne and Its Family under Elastic Strain: Theoretical Predictions. *J. Phys. Chem. C* **2013**, *117*, 14804−14811.
(20) Gao, X.; Zhu, Y.; Yi, D.; Zhou, J.; Zhang, S.; Yin, C.; Ding, F.; Zhang, S.; Yi, X.; Wang, J.; Tong, L.; Han, Y.; Liu, Z.; Zhang, J. Ultrathin Graphdiyne Film on Graphene through Solution-Phase Van Der Waals Epitaxy. *Sci. Adv.* **2018**, *4*, No. eaat6378.
(21) Zhou, J.; Xie, Z.; Liu, R.; Gao, X.; Li, J.; Xiong, Y.; Tong, L.; Zhang, J.; Liu, Z. Synthesis of Ultrathin Graphdiyne Film Using a Surface Template. *ACS Appl. Mater. Interfaces* **2019**, *11*, 2632−2637.
(22) Li, J.; Xiong, Y.; Xie, Z.; Gao, X.; Zhou, J.; Yin, C.; Tong, L.; Chen, C.; Liu, Z.; Zhang, J. Template Synthesis of an Ultrathin β-Graphdiyne-Like Film Using the Eglinton Coupling Reaction. *ACS Appl. Mater. Interfaces* **2019**, *11*, 2734−2739.
(23) Kan, X.; Ban, Y.; Wu, C.; Pan, Q.; Liu, H.; Song, J.; Zuo, Z.; Li, Z.; Zhao, Y. Interfacial Synthesis of Conjugated Two-Dimensional N-Graphdiyne. *ACS Appl. Mater. Interfaces* **2018**, *10*, 53−58.
(24) Matsuoka, R.; Sakamoto, R.; Hoshiko, K.; Sasaki, S.; Masunaga, H.; Nagashio, K.; Nishihara, H. Crystalline Graphdiyne Nanosheets Produced at a Gas/Liquid or Liquid/Liquid Interface. *J. Am. Chem. Soc.* **2017**, *139*, 3145−3152.
(25) Li, W.; Liu, J.; Yu, Y.; Feng, G.; Song, Y.; Liang, Q.; Liu, L.; Lei, S.; Hu, W. Synthesis of Large-Area Ultrathin Graphdiyne Films at an Air−Water Interface and Their Application in Memristors. *Mater. Chem. Front.* **2020**, *4*, 1268−1273.
(26) Dean, C. R.; Young, A. F.; Meric, I.; Lee, C.; Wang, L.; Sorgenfrei, S.; Watanabe, K.; Taniguchi, T.; Kim, P.; Shepard, K. L.; Hone, J. Boron Nitride Substrates for High-Quality Graphene Electronics. *Nat. Nanotechnol.* **2010**, *5*, 722−726.
(27) Britnell, L.; Gorbachev, R. V.; Jalil, R.; Belle, B. D.; Schedin, F.; Mishchenko, A.; Georgiou, T.; Katsnelson, M. I.; Eaves, L.; Morozov, S. V.; Peres, N. M. R.; Leist, J.; Geim, A. K.; Novoselov, K. S.; Ponomarenko, L. A. Field-Effect Tunneling Transistor Based on Vertical Graphene Heterostructures. *Science* **2012**, *335*, 947−950.
(28) Jo, S.-H.; Kang, D.-H.; Shim, J.; Jeon, J.; Jeon, M. H.; Yoo, G.; Kim, J.; Lee, J.; Yeom, G. Y.; Lee, S.; Yu, H.-Y.; Choi, C.; Park, J.-H. A High-Performance WSe_2/h-BN Photodetector Using a Triphenylphosphine (PPh_3)-Based N-Doping Technique. *Adv. Mater.* **2016**, *28*, 4824−4831.
(29) Seo, S.; Jo, S.-H.; Kim, S.; Shim, J.; Oh, S.; Kim, J.-H.; Heo, K.; Choi, J.-W.; Choi, C.; Oh, S.; Kuzum, D.; Wong, H. S. P.; Park, J.-H. Artificial Optic-Neural Synapse for Colored and Color-Mixed Pattern Recognition. *Nat. Commun.* **2018**, *9*, 5106.
(30) Cheng, R.; Wang, F.; Yin, L.; Wang, Z.; Wen, Y.; Shifa, T. A.; He, J. High-Performance, Multifunctional Devices Based on Asymmetric Van Der Waals Heterostructures. *Nat. Electron.* **2018**, *1*, 356−361.
(31) Huang, W.; Yin, L.; Wang, F.; Cheng, R.; Wang, Z.; Sendeku, M. G.; Wang, J.; Li, N.; Yao, Y.; Yang, X.; Shan, C.; Yang, T.; He, J. Multibit Optoelectronic Memory in Top-Floating-Gated Van Der Waals Heterostructures. *Adv. Funct. Mater.* **2019**, *29*, 1902890.
(32) Kim, S. H.; Yi, S.-G.; Park, M. U.; Lee, C.; Kim, M.; Yoo, K.-H. Multilevel MoS_2 Optical Memory with Photoresponsive Top Floating Gates. *ACS Appl. Mater. Interfaces* **2019**, *11*, 25306−25312.
(33) Danial, L.; Pikhay, E.; Herbelin, E.; Wainstein, N.; Gupta, V.; Wald, N.; Roizin, Y.; Daniel, R.; Kvatinsky, S. Two-Terminal Floating-Gate Transistors with a Low-Power Memristive Operation Mode for Analogue Neuromorphic Computing. *Nat. Electron.* **2019**, *2*, 596.
(34) Tran, M. D.; Kim, H.; Kim, J. S.; Doan, M. H.; Chau, T. K.; Vu, Q. A.; Kim, J.-H.; Lee, Y. H. Two-Terminal Multibit Optical Memory Via Van Der Waals Heterostructure. *Adv. Mater.* **2019**, *31*, 1807075.
(35) Deng, B.; Pang, Z.; Chen, S.; Li, X.; Meng, C.; Li, J.; Liu, M.; Wu, J.; Qi, Y.; Dang, W.; Yang, H.; Zhang, Y.; Zhang, J.; Kang, N.; Xu, H.; Fu, Q.; Qiu, X.; Gao, P.; Wei, Y.; Liu, Z.; Peng, H. Wrinkle-Free Single-Crystal Graphene Wafer Grown on Strain-Engineered Substrates. *ACS Nano* **2017**, *11*, 12337−12345.
(36) Pan, Z.; Liu, N.; Fu, L.; Liu, Z. Wrinkle Engineering: A New Approach to Massive Graphene Nanoribbon Arrays. *J. Am. Chem. Soc.* **2011**, *133*, 17578−17581.
(37) Yang, L.-L.; Wang, H.-J.; Wang, J.; Li, Y.; Zhang, W.; Lu, T.-B. A Graphdiyne-Based Carbon Material for Electroless Deposition and Stabilization of Sub-Nanometric Pd Catalysts with Extremely High Catalytic Activity. *J. Mater. Chem. A* **2019**, *7*, 13142−13148.
(38) Song, X.; Gao, J.; Nie, Y.; Gao, T.; Sun, J.; Ma, D.; Li, Q.; Chen, Y.; Jin, C.; Bachmatiuk, A.; Rümmeli, M. H.; Ding, F.; Zhang, Y.; Liu, Z. Chemical Vapor Deposition Growth of Large-Scale Hexagonal Boron Nitride with Controllable Orientation. *Nano Res.* **2015**, *8*, 3164−3176.
(39) Li, Y.; Zhang, M.; Hu, X.; Fan, X.; Yu, L.; Huang, C. Light and Heat Triggering Modulation of the Electronic Performance of a Graphdiyne-Based Thin Film Transistor. *J. Phys. Chem. Lett.* **2020**, *11*, 1998−2005.
(40) Luo, G.; Qian, X.; Liu, H.; Qin, R.; Zhou, J.; Li, L.; Gao, Z.; Wang, E.; Mei, W.-N.; Lu, J.; Li, Y.; Nagase, S. Quasiparticle Energies and Excitonic Effects of the Two-Dimensional Carbon Allotrope Graphdiyne: Theory and Experiment. *Phys. Rev. B: Condens. Matter Mater. Phys.* **2011**, *84*, 075439.
(41) Zhou, J.; Gao, X.; Liu, R.; Xie, Z.; Yang, J.; Zhang, S.; Zhang, G.; Liu, H.; Li, Y.; Zhang, J.; Liu, Z. Synthesis of Graphdiyne Nanowalls Using Acetylenic Coupling Reaction. *J. Am. Chem. Soc.* **2015**, *137*, 7596−7599.
(42) Zheng, Q.; Luo, G.; Liu, Q.; Quhe, R.; Zheng, J.; Tang, K.; Gao, Z.; Nagase, S.; Lu, J. Structural and Electronic Properties of Bilayer and Trilayer Graphdiyne. *Nanoscale* **2012**, *4*, 3990−3996.
(43) Qian, X.; Liu, H.; Huang, C.; Chen, S.; Zhang, L.; Li, Y.; Wang, J.; Li, Y. Self-Catalyzed Growth of Large-Area Nanofilms of Two-Dimensional Carbon. *Sci. Rep.* **2015**, *5*, 7756.
(44) Lee, D.; Hwang, E.; Lee, Y.; Choi, Y.; Kim, J. S.; Lee, S.; Cho, J. H. Multibit MoS_2 Photoelectronic Memory with Ultrahigh Sensitivity. *Adv. Mater.* **2016**, *28*, 9196−9202.
(45) Li, D.; Chen, M.; Zong, Q.; Zhang, Z. Floating-Gate Manipulated Graphene-Black Phosphorus Heterojunction for Nonvolatile Ambipolar Schottky Junction Memories, Memory Inverter Circuits, and Logic Rectifiers. *Nano Lett.* **2017**, *17*, 6353−6359.
(46) Cheng, R.; Wang, F.; Yin, L.; Xu, K.; Ahmed Shifa, T.; Wen, Y.; Zhan, X.; Li, J.; Jiang, C.; Wang, Z.; He, J. Multifunctional Tunneling Devices Based on Graphene/h-BN/$MoSe_2$ Van Der Waals Heterostructures. *Appl. Phys. Lett.* **2017**, *110*, 173507.
(47) Liu, C.; Yan, X.; Wang, J.; Ding, S.; Zhou, P.; Zhang, D. W. Eliminating Overerase Behavior by Designing Energy Band in High-Speed Charge-Trap Memory Based on WSe_2. *Small* **2017**, *13*, 1604128.
(48) Ji, Y.; Pan, C.; Zhang, M.; Long, S.; Lian, X.; Miao, F.; Hui, F.; Shi, Y.; Larcher, L.; Wu, E.; Lanza, M. Boron Nitride as Two Dimensional Dielectric: Reliability and Dielectric Breakdown. *Appl. Phys. Lett.* **2016**, *108*, 012905.
(49) Schedin, F.; Geim, A. K.; Morozov, S. V.; Hill, E. W.; Blake, P.; Katsnelson, M. I.; Novoselov, K. S. Detection of Individual Gas Molecules Adsorbed on Graphene. *Nat. Mater.* **2007**, *6*, 652−655.
(50) Lee, G.-H.; Yu, Y.-J.; Lee, C.; Dean, C.; Shepard, K. L.; Kim, P.; Hone, J. Electron Tunneling through Atomically Flat and Ultrathin Hexagonal Boron Nitride. *Appl. Phys. Lett.* **2011**, *99*, 243114.

https://dx.doi.org/10.1021/acsami.0c05327
ACS Appl. Mater. Interfaces 2020, 12, 33069−33075